Regional-scale correlation between CO_2 fire emissions, burned areas, and mid-tropospheric CO_2 diurnal variations over southern Africa

A. Chédin[1*], N. A. Scott,[1] P. Ciais[2], C. Rio[3], F. Hourdin[3], C. Crevoisier[1], R. Armante[1]

[1] {Laboratoire de Météorologie Dynamique, IPSL, Ecole Polytechnique, 91128 Palaiseau, France}

[2] {LSCE, UMR CEA-CNRS, CE, L'Orme des Merisiers, Gif-sur-Yvette, France}

[3] {Laboratoire de Météorologie Dynamique, IPSL, Université P. et M. Curie, 75252 Paris, France}

Correspondence to: A. Chédin (chedin@lmd.polytechnique.fr)

Abstract

The mid-troposphere diurnal anomaly observed from space between evening and morning CO_2 columns is investigated at regional scale for ten regions of southern Africa with the aim of analyzing its properties as a proxy of fire emission. A possible mechanism for CO_2 concentration being higher in the evening than in the morning is that hot convective fire plumes inject emissions directly into the troposphere during the afternoon peak of fire activity, seen by the satellite in the evening, and then diluted by large-scale atmospheric transport before the next satellite pass in the morning. 3D simulations of this "Daily Tropospheric Excess (DTE)" by the LMDz General Circulation Model, in which a pyro-thermal plume model is activated, confirm the observations. A large fraction of fire products is directly injected in the mid-troposphere, well above the boundary layer. This rapid uplift of CO_2, combined with atmospheric transport patterns in southern Africa during the dry season, characterized by a fluctuating continental gyre, produces a daily DTE signal mainly positive above the source region and either positive or negative outside of the source region. On a monthly mean, this results in a persistent DTE signal above the source

region of an order of 1ppm, while the impact of large-scale advection vanishes. The DTE signal is then compared with other datasets that have been used to estimate burned area and fire emissions (GFEDv2, the Global Fire Emission Database version 2, and L3JRC of the Joint Research Center) and shows similar seasonal and annual patterns. DTE also displays regional scale interannual variability which correlates well with ENSO, as do fire emissions themselves. We conclude that the DTE signal might represent a quantitative proxy of fire emission spatial patterns, in particular before the ATSR or MODIS observation periods when better quality fire count and burned area data became available.

1 Introduction

Biomass burning is a large source of atmospheric CO_2, CO, aerosols and chemically important trace gases and a major component of the carbon cycle and Earth climate system. Average annual carbon emissions from fires are around 2.5 Pg C $year^{-1}$ with African emissions accounting for 50% of the total, equally distributed over both hemispheres (van der Werf et al., 2006). However, estimates of CO_2 emissions from fires still suffer from large uncertainties. In particular, the relationship between emissions, climate and human activities is still uncertain. This is particularly true for tropical fires which are suspected to cause most of the year-to-year variability in the growth rate of atmospheric CO_2 and other key species (e.g. Langenfelds et al., 2002; van der Werf et al., 2004). Within the tropics, savanna fires alone contribute roughly 20% of the emissions (Andreae, 1996). This large source of CO_2 associated to savanna fires is highly seasonal and it is offset during the wet season by CO_2 uptake associated to re-growth. The extent to which savanna ecosystems are today carbon neutral with respect to fires is unknown, although there is some evidence that savanna fires have increased during the 20^{th} century in response to rising population (Mouillot and Field, 2005; Crutzen and Zimmermann, 1991; van Aardenne et al., 2001).

Numerical simulations suggest a moderate effect of biomass burning on the CO_2 seasonal cycle, as measured at the global network of marine stations (Wittenberg et al., 1998; van der Werf et al., 2004) but a large impact on the interannual growth rate variability (Langenfelds et al., 2002; van der Werf et al., 2004, Patra et al., 2005). However, the scarcity of surface stations implies that the tropical carbon balance remains largely un-constrained. Moreover, interannual variations of reactive species such as CO, CH_4, H_2 have been observed to closely correlate with those of CO_2 (Langenfelds et al., 2002). This suggests that climate induced fluctuations of fire emissions play a major role in the

variability of tropical and global atmospheric chemistry. In that context, any knowledge of fire emissions derived from CO_2 atmospheric observations has also great potential to deliver a better understanding of the cycles of reactive species.

The amount of CO_2 released to the atmosphere by fire is generally estimated as the product of burned area by fuel loads and combustion completeness. Burned area is considered to be the most uncertain parameter in emission estimates on a global scale (Mouillot and Field, 2005; Palacios-Orueta et al., 2005; van der Werf et al., 2006). Burned area is usually derived from satellite observations (Barbosa et al., 1999; Schultz, 2002; Duncan et al., 2003; Ito and Penner, 2004; Kasischke and Penner, 2004; Hoelzemann et al., 2004; van der Werf et al., 2006; Giglio et al., 2006a-b; Tansey et al., 2008a), and used as an input of fire modules in vegetation models (van der Werf et al., 2003, 2004; Randerson et al., 2005).

Maps of fire emissions derived from satellite observations of fire hot spots (counts) or burned scars remain highly uncertain. Moreover, the burned-area-based approach to estimate emissions is limited to the time period of adequate satellite observations, typically the past 10 years. This hampers diagnostic of the long-term evolution of fires, as well as projection of future trends and understanding of fire/climate relationships.

Recently, global observations of upper-air CO_2 have become available from space-borne infrared sounders, providing information on the variation of its concentration (seasonal, interannual, trend), in the tropical mid-troposphere. Monthly mean CO_2 columns have been retrieved from evening (1930 LST) and morning (0730 LST) observations of the TOVS instruments flying onboard the NOAA polar satellites (Chédin et al., 2002, 2003a-b). A strong correlation (R^2~0.8) was found between CO_2 emissions from the Global Fire Emission Dataset, version 2 (GFEDv2; Randerson et al. 2006) and the difference between evening minus morning column CO_2 from TOVS, hereafter called Daily Tropospheric Excess (DTE). It was shown that the DTE exhibits continental-scale spatio-temporal patterns that are in good agreement with burned-area based CO_2 emissions over most of the tropical regions affected by fires (Chédin et al., 2005, 2008). It was also shown that DTE displays interannual variability which correlates well with ENSO, as for fire emissions themselves (Chédin et al., 2008). The DTE signal could thus be used as a proxy of CO_2 emissions to reconstruct fire emission before the ATSR and MODIS era. Burned area data could also benefit from constraints brought by DTE observations derivable from the new generation sounder Infrared Atmospheric Sounder Interferometer (IASI) operational since 2006.

The correlation between DTE and fire emissions in tropical regions seems to be related to the strong diurnal cycle affecting fires (Giglio, 2007, Roberts et al., 2009). A possible mechanism for CO_2 concentration being higher in the afternoon than in the morning is that hot convective fire plumes inject emissions directly into the troposphere during the afternoon peak of fire activity, seen by the satellite at 1930LST, and then diluted by large-scale atmospheric transport before the next satellite pass at 0730LST. Even if no direct observations have confirmed the existence of such a mechanism over southern Africa, several studies bring some credibility to it. In particular, Rio et al. (2009, this issue) simulate a DTE signal of an order of 1 ppm over southern Africa by including a scheme for pyro-convection, the "pyro-thermal plume model", in the General Circulation Model (GCM) LMDz (Hourdin et al., 2006), and Freitas et al. (2007), using a regional model including the representation of the transport by convective plumes generated by fires, simulate injection heights reaching 7 km over southern Africa. Chédin et al. (2008) found high positive correlations between DTE and tropical fire emissions at continental scale in Africa but they did not investigate correlations at regional scale, a relevant scale at which vegetation cover and fire susceptibility relationships might become more homogeneous and for which eventual compensation phenomena are less likely to occur.

We present in this paper a regional-scale analysis of the DTE distribution inferred from NOAA-10 over ten regions of southern hemisphere Africa from 1987 to 1991 (sections 2.1 and 2.2). Results from simulations by the LMDz GCM including the pyro-thermal plume model of Rio al. (2009, this issue) are further analyzed to investigate the credibility of the mechanisms suggested by the observations as responsible for this tropospheric excess (sections 2.3). Comparisons are then made between DTE and two fire CO_2-emission datasets: the Global Fire Emission Dataset, version 2 (GFEDv2; Randerson et al., 2006) covering the period 1997-2004, and the global burnt areas dataset of the Joint Research Center (L3JRC) (Tansey et al., 2008a) covering the period 2000-2007. These comparisons show that there is a quantitative link between the DTE and CO_2 emissions retrieved by independent measurements, suggesting that the DTE signal could be used to deduce CO_2 emissions from biomass burning. Conclusions are drawn in section 4.

2 The Daily Tropospheric Excess of CO_2: an indicator of fire activity

2.1 An intense burning region: Africa

Africa represents some 50% of the total fire emissions - roughly evenly distributed into both hemispheres. It is probably the continent for which fire activity has been studied most in depth. Therefore, there are different fire emission related datasets (emissions, burned areas, etc.). Due to a strong and rather long dust aerosol season, partly overlapping with the dry fire season, northern Africa (NAF) is less suitable to a regional-scale study of CO_2 from space observations than is southern Africa (SAF). As reported by van der Werf et al. (2006), if emissions from SAF (~ 580 Tg C year^{-1}) are somewhat smaller than emissions from NAF (~ 630 Tg C year^{-1}), the average fuel consumption appears to be higher in SAF. This is because of more woodland fires in SAF, against savannas fires in NAF.

Following Hoelzemann (2006), SAF has been divided into 10 sub-regions with different vegetation characteristics (Mayaux et al., 2004; DeFries et al., 1998). This is illustrated in Figure 1. Region 1 is dominated by tropical forests; region 2 by grasslands with some forests, woodlands and shrublands; regions 3 and 5 by closed deciduous forests and mosaic forest/savanna. Woodlands and shrublands dominate regions 4 and 6. Grasslands dominate region 7. Both woodlands and grasslands dominate region 8. Region 9 is a mix of woodlands, croplands, grasslands and forests and region 10 of grasslands, shrublands and mosaic forest/savanna. Additionally, we define two larger regions, called ASs (south of 14S) and ASn (north of 14S), covering the southern and the northern parts of southern Africa respectively (Table 1). In both GFEDv2 (CO_2 emissions) and L3JRC (burnt areas) datasets, the highest relative contributors to SAF emissions are regions 3, 5, 4 and 6 - in this order - i.e. the four regions with higher woody vegetation coverage.

2.2 Observed diurnal anomaly of CO_2 in the troposphere

Flying aboard the National Oceanic and Atmospheric Administration (NOAA) polar meteorological satellites since 1978 (Smith et al., 1979), the TOVS instrument consists of the High resolution Infrared Radiation Sounder (HIRS-2), the Microwave Sounding Unit (MSU) and the Stratospheric Sounding Unit (SSU). In the 15 μm and 4.3 μm spectral bands, HIRS-2 radiances mostly depend on the temperature of the atmosphere but also, although weakly (Chédin et al., 2002), on the CO_2 concentration. The MSU observations are also sensitive to temperature, but are insensitive to CO_2. Combining HIRS-2 and MSU allows separating the two signals. The approach developed by Chédin et al. (2003a, 2005, 2008) to retrieve CO_2 is based upon a non-linear regression inverse radiative transfer model based on the Multi-Layer Perceptron (Rumelhart et al., 1986) and was applied to NOAA-10 observations.

The retrieved CO_2 columns are weighted to the tropical mid-troposphere with a peak sensitivity at ~300 hPa, half the peak sensitivity at ~120 hPa and ~600 hPa, and no sensitivity to the surface (see Fig 1 in Chédin et al., 2003a). Mid-tropospheric CO_2 columns were retrieved from NOAA-10 observations at 0730 LST (daytime) and 1930 LST (nighttime), between January 1987 and August 1991, in the tropical zone (30N-30S) where most of the biomass burning emissions are located. This period is marked by the end of the 1986-1987 El Nino, followed by a strong La Nina episode in 1988-1989, and by the beginning of a weak El Nino at the end of 1990 (see discussion in Chédin et al. (2005, 2008)).

In the present study, individual daily CO_2 column retrievals are produced at a spatial resolution of 1°x1°. Morning and evening CO_2 retrievals are then collocated: within a 1°x1° grid box, a morning daily CO_2 retrieval is retained only if an evening retrieval is found during the same day. If this collocation criterion is met, the difference between the evening and the morning CO_2 retrievals is formed, which defines one item of the 1°x1° DTE data set. Oppositely, if the collocation is not met, the CO_2 retrieval is rejected. These individual DTE items are then averaged temporally over a month. Areas with no data reflect the presence of a persistent cloudiness. As shown in Chédin et al. (2008), the DTE monthly mean accuracy is of the order of 0.4-0.5 ppm (see details in this reference). This relatively good accuracy is due to the nature of this variable. Being differential, it is almost insensitive to instrumental or platform (drift) problems and show a low sensitivity to the two main potential sources of contamination that are ozone and aerosols. Moreover, the burning season in SAF is characterized by rather low levels of such contaminants (Ziemke et al., 2006; Bryant et al., 2007).

As shown by Chédin et al. (2008), the striking DTE property is the existence of regional maxima of several ppm over areas affected by fires. This is illustrated for SAF by Figure 2 (a-d) which displays four year averaged seasonal DTE maps. The DTE patterns shown by this figure are in agreement with the fire counts analysis of Cahoon et al. (1992) who described the west-to-east displacement of fires between March and November, due to drier conditions spreading from Namibia to the East. In May, biomass burning is widespread into SAF western and interior regions. In June, it peaks over the southern part of the Democratic Republic of Congo. From July to October, biomass burning spreads to the East and wanes in western and interior regions. Finally, from November to December, fires persist along the eastern coast of SAF (Kenya, Tanzania) and cease in December. At continental-scale, the seasonal variability of DTE was already characterized to be in good

agreement (R^2~0.8) with GFEDv2 fire CO_2 emissions. Characteristic inter-annual changes in fire activity during the transition from El Niño to La Niña were also found to be in agreement between the DTE and GFEDv2 products, despite the different El Niño-to-La Niña transitions covered by each dataset.

2.3 Mechanisms responsible for this tropospheric excess: a numerical study

In this section we use 3D simulations performed with the General Circulation Model LMDz (Hourdin et al., 2006) to assess the credibility of the proposed mechanisms to explain the observed DTE.

2.3.1 Simulating pyro-convection in a General Circulation Model

The GCM includes a parameterization of convective plumes generated by the excess of buoyancy associated with fires, as proposed by Rio et al. (2009, this issue). In the so-called "pyro-thermal plume" model, the plume is driven by the heat flux released by the fire and its vertical evolution depends on the area covered by the plume as well as on environmental conditions. The transport of CO_2 emitted by biomass burning over southern Africa in July is simulated using monthly mean CO_2 emissions (see Fig.7 of Rio et al., 2009) derived from observations gathered during the AMMA field campaign in July 2006 (Liousse et al., 2009). At the beginning of the simulation, the atmosphere is CO_2 free. Within a grid cell, CO_2 daily emission is taken constant throughout the month, with a simple specification of the diurnal cycle: the heat flux and the CO_2 flux released from the surface are assumed to follow a Gaussian time-profile centered on 15:45 LST with a standard deviation of 1 hour. The maximum heat flux value is set to 80 kJ m^{-2}. The active burned area for one fire is set to 2 km^2. The simulation allows reproducing CO_2 emitted by fires separately, a signal which can not be distinguished from background CO_2 in the DTE observations. The pyro-thermal plume model allows simulating the vertical transport of the emitted CO_2 by convection induced by the fires themselves.

2.3.2 Model results for DTE

Applying the weighting function of satellite retrieval to the simulated CO_2 concentration on the vertical allows analysing the CO_2 concentration which would be seen from space at different times of the day. Figure 3 shows the simulated integrated concentration of CO_2 from biomass burning as would be seen by TOVS at 7am and 7pm for four consecutive days of July. The evening minus morning DTE difference, computed from the difference

between those two concentrations, is also shown. On a daily scale, the modelled DTE signal can be negative over parts of the source region, indicating a higher concentration in the morning than in the evening. Negative daily DTE can also be modelled around the fire source region. In the simulation, since fire emissions are assumed homogeneous, the modelled DTE variations can only be caused by atmospheric circulation processes. Horizontal winds at 500 hPa averaged over night are drawn upon the modelled CO_2 at 7am, and afternoon winds upon modelled CO_2 at 7pm.

On the 18th of July (day 1), westerlies from the ocean turn from South-East to North-West when reaching the coast transporting CO_2 from the source region towards the South-East, causing CO_2 accumulation over South Africa and the nearby ocean, leading to a positive DTE there. During the 19th of July in the afternoon (day 2), winds from the Atlantic ocean penetrate over South Africa, ventilating the CO_2 accumulated south of 15S, which explains the negative DTE signal over land and the positive signal along the eastern coast south of 15S that day. On the 20th of July (day 3), north-westerlies transport CO_2 to the South-East, which explains why the DTE signal is of opposite sign to that of the day before over ocean.

On the 21st of July (day 4), the negative DTE signal between 15S and 25S over land is due to southerly winds which transport CO_2 present there at 7am to the north during the afternoon. This shows that the variability of DTE from day to day can largely be ascribed to wind fields.

Fires weakly affect the CO_2 seasonal cycle, implying that biomass burning CO_2 does not accumulate locally in the mid-troposphere, but gets advected away from the source region. Figure 4 shows the monthly evolution of CO_2 from biomass burning modelled at 7am and at 7pm (left) and of the corresponding DTE signal (right) above 3 points in Southern Africa at 20E-20S, 20E-10S, 20E-5S respectively. At 20E-10S, the point located in the center of the fire region, the integrated CO_2 concentration rises rapidly at the beginning of the simulation up to around 2 ppm. On the 20th of July, CO_2 rises again before stabilizing at 3 ppm. This evolution is associated with DTE which stays positive but varies from day to day, ranging from 0.2 to 1.5 ppm. At the points located at 20S and 5S near the boundary of the fire region, the CO_2 signal is much noiser. DTE is either positive or negative depending on the day. Those results show that outside the source region, the daily DTE variations more or less cancel each other on a monthly basis. Over the center of the source region oppositely, DTE is mostly positive, but can still vary by 1 ppm from day to day. The monthly mean DTE for this simulation is indeed shown in Rio & al. (2009, this issue): the signal is persistent only over the source region, with values reaching 1ppmv. Moreover,

Rio & al. (2009) shows that this DTE signal cannot be recovered if the pyro-thermal plume model is activated, emissions staying confined within the boundary layer.

The simulated DTE distribution histogram is presented in Figure 5 for the two large regions ASn and ASs. These two distributions peak at positive DTE values, but there is a significant tail of negative values. Region ASs has more negative values than ASn and less positive values. Figure 6 shows the distributions of the observed DTE for the same two regions. Simulated and observed distributions both peak at positive DTE values, with ASs having more negative values than ASn and less positive values. Yet, comparing observed and simulated DTE distributions is not straightforward because the simulation assumes the same emissions each day over July while in the real world, fires vary from day to day. In addition, variable background CO_2 and noise from the instrument, retrieval method and from remaining interferences (e.g. undetected thin clouds) enter into the observed DTE distribution. This difference explains the larger width of the observed distributions. Moreover, the observed DTE signal remains larger on average than the model simulations. Figs. 5 and 6 imply that with the DTE signal resulting from fires is associated a "noise" due to transport (mostly advection). This "noise" possibly causes too small DTE in the morning and too high DTE in the evening. Averaging over a month, the signal sorts out from the noise. Compensation phenomena between abnormally low and abnormally high DTE values approximately maintain the quantitative relationship observed between DTE and emission related products.

2.3.3 Discussion

The results of the 3D simulation of DTE essentially confirm the hypothesis raised from observations:

- fire emissions products are transported vertically by fires induced convection, potentially to the mid-troposphere where it can be seen by the satellite;

- fire emissions are then further advected by large-scale winds, which explains why the DTE signal contains negative values, particularly south of 15S outside the fire region. Atmospheric circulation patterns over southern Africa in the dry season are characterized by a semi permanent continental gyre throughout the troposphere, particularly south of 10S, with easterly winds in the tropical band (10S–20S), westerly winds in the southern sub-tropical band (20S–30S), and meridional winds over the east and west coasts of Africa at around 20S. On average, this continental gyre prevails approximately half the time during the dry season and is perturbed by westerly waves roughly 30% of the time (Sinha

et al., 2003; Jury, 2000). This recirculation pattern opens the possibility for observing morning columns containing more fire emissions than evening columns, i.e. negative DTE. This circulation also can cause afternoon columns to be charged in emissions more than once a day, resulting into higher DTE. As observed and simulated, the DTE is thus not systematically positive but also takes negative values, even though the monthly mean value remains positive over fire regions.

Two recent studies, one based on observations and one based on simulations confirm our findings. Coheur et al. (2007) using observations from the solar occultation infrared Atmospheric Chemistry Experiment/Fourier Transform Interferometer (ACE/FTS) analyzed a remarkable plume event near the East coast of Tanzania in early October 2005. That plume is characterized by a strong CO concentration enhancement above a background value of about 70-80 ppbv, with a peak value of more than 160 ppbv at about 220 hPa. Their analysis demonstrates that the dominant contribution to the total upper air CO comes from African biomass burning and to a lesser extent from anthropogenic emissions. The plume sampled by the ACE-FTS is young and likely originated from a relatively nearby fire. Freitas et al. (2006, 2007) describe a parameterization to include the vertical transport of hot gases emitted from biomass burning into coarse resolution atmospheric-chemistry-transport models. Their method consists of embedding a 1-D cloud-resolving model in each column of the larger-scale host model. They showed the effect of their "plume rise mechanism" on the vertical distribution of CO. Without plume rise, CO would remain confined into the boundary layer. With it, the boundary layer is polluted by emissions from the smoldering phase whereas a large excess of CO produced during the flaming phase is delivered at about 8 km altitude (Fig. 7 of Freitas et al., 2007). These examples, among others, confirm the mechanism of a rapid uplift and transport of biomass burning emitted CO_2 in the tropical mid-troposphere.

3 The Daily tropospheric Excess of CO2: a quantitative proxy of fire emissions?

As the DTE is related to the vertical transport of fire emissions, the question of whether or not DTE is a proxy of fire activity at regional scale is now addressed by comparing it to two datasets established specifically to quantify fire emissions: 1) the GFEDv2 emission dataset based upon MODIS burned area data encapsulated into the Carnegie Ames Stanford Approach (CASA) biogeochemical model (Potter et al., 1993; Randerson et al., 1996), and

2) the L3JRC-global burned areas dataset based upon SPOT-Vegetation burned areas (Tansey et al., 2008a). Comparisons only include grid points of 1° by 1° in which there is a fire signal. This is defined by CO_2 emissions higher than 1 g CO_2 m^{-2} in GFEDv2 and burned fractions greater than 0.002 in L3JRC. Similarly, grid points with DTE values within the interval ± 0.3 ppm (see section 4) are discarded.

3.1 Fire emission related products

The GFEDv2 dataset covers the period 1997-2004 at a resolution of 1°x1°. The L3JRC dataset covers the period 2000-2007 (March 2007) at a spatial resolution of 1 km. Here, we used data averaged at 1°x1°. Lehsten et al. (2009) corrected the L3JRC burned area estimates for the bias introduced by low-resolution observations, and accounting for the standard deviation observed around the best-fit line when compared to a number of Landsat TM images. These improvements, not included in the L3JRC dataset used here, do not affect the seasonal cycle comparisons. Obviously, comparison with DTE observed during the period 1987-1991 is limited by the different time span of observations. However over SAF, interannual changes and trends remain relatively small compared to yearly mean values and seasonal amplitudes (van der Werf et al., 2008).

3.2 A quantitative relationship at regional scale

3.2.1 Annual scale, spatial correlation between DTE and other fire products

Figure 7 compares DTE in ppm, with GFEDv2 emissions in g CO_2 m^{-2}, across the 12 SAF regions of Table 1. Each value is an average over the whole period of observation. A very tight linear relationship can be seen between the two variables (1 ppm DTE approximately corresponds to 25 g CO_2 m^{-2}) over a large range of emission variation (from 18 to 80 g CO_2 m^{-2}). This tight relationship supports the use of DTE as a proxy of fire activity. Regions 3, 5, 4 and 6, as well as the northern part of SAF (ASn) have the highest values. Region 3 has smaller DTE compared to CO_2 emissions, because of few local extremely high values appearing in GFED data. The atmospheric signature of such intense localized fires is smoothed out by the spatial resolution of the TOVS observations (also, the period of observation is different). Region 7 covering southern Angola and northern Namibia shows lower DTE values than GFEDv2 emissions. This region is dominated by grasslands ecosystems with low fuel loads and emissions. It is also characterized by a relatively large

interannual variability (van der Werf et al., 2008; see also next paragraph). Altogether, having in mind the uncertainties in the two products, the agreement between DTE and GFED appears quite good.

3.2.2 Interannual variability

Figure 8 shows annual means of DTE (Fig. 8a), L3JRC burned area fractions (Fig. 8b), and GFEDv2 emissions (Fig. 8c) for the regions of study, normalized by their means over their respective periods of coverage. Deviations from unity define interannual variability (IAV) in each dataset. Obviously, the IAV of DTE must be taken with care as only 4 years are available, with an El Nino / La Nina couple. Fig.8 shows several interesting features: (1) the low IAV of L3JRC compared to the other two products; (2) the IAV similarities between DTE and GFEDv2, however with exceptions probably due to the too short period covered by DTE. For example, in region 8, the DTE variability entirely depends on the abnormal year 1990 marked by large emissions (Barbosa et al, 1999). In agreement with GFEDv2, the IAV of DTE over forested regions is smaller than over the savannas (see also Ciais et al., 2008). However, because emissions from forested regions are larger in absolute value (see red dashed line on Fig. 8c) they still dominate the overall IAV.

The African continent shows a large IAV in carbon balance resulting primarily from climatic perturbations related to El Nino that directly affects the ecosystems productivity and the fire activity (Weber et al., 2009 and references herein, Ciais et al., 2008). Figure 9 compares the 1998 to 1999 fire emission ratio in GFEDv2, with 1987 to 1988 ratio in DTE. These pairs of years have the same sequence of an El Nino (1987 and 1998) followed by a La Nina episode (1988 and 1999). These pairs also show large similarities (not shown) in the precipitation patterns for the two-year periods preceding and including the peak fire month used to estimate precipitation levels during the period when herbaceous fuels typically accumulate (van der Werf et al., 2008; precipitations fields from Mitchell et al., 2005, http://www.cru.uea.ac.uk/cru/data/hrg.htm). However, exceptions are clearly seen for regions 8 and 10 (not shown) and could explain why DTE and GFED disagree. Note also that regions 8 and 9 are regions where precipitation has greatest interannual variability in southern Africa, and thus vegetation also has greatest variability (Weber et al., 2008).

A relatively good agreement is seen between DTE and GFEDv2 ratios. For example, one can see values above unity for the eastern regions 4 and 6. This result is coherent with conclusions from Anyamba et al. (2003) or Weber et al. (2009). On the contrary, the ratios disagree for region 8 between DTE and GFEDv2, the reason being an abnormal DTE value

for year 1990 and for region 10 characterized by the highest interannual variability in both the DTE and the GFEDv2 data sets (see Fig. 8). Going further into the interpretation of these results is hindered by the fact that fire activity IAV is not always related to climate and vegetation: other factors are equally important because fire has largely become a human-driven phenomenon in the tropics and subtropics (van der Werf et al, 2008; Archibald et al., 2009).

3.2.3 Seasonal scale

The seasonal cycles are now compared between DTE and the two other datasets. Figure 10 compares monthly GFEDv2, L3JRC, and DTE seasonal cycles for the 10 regions of SAF and for the two larger regions ASn and ASs. If the overall agreement is relatively satisfactory, this comparison brings into evidence two types of regional behaviour. Over regions 1 to 5, the seasonal cycles are approximately in phase between DTE and the other two products, yet with a too short fire season in regions 1 and 2. This is due to cloudiness which precludes getting reliable DTE results in May and August. In regions 3 and 5 (although to a lesser extent), the DTE relative seasonal amplitude is smaller than in GFEDv2 and L3JRC which both contain few local extremely high values. For both regions, GFEDv2 (or L3JRC) data larger than the mean + 2.5 σ (σ = standard deviation of the distribution) have been rejected because the lower spatial resolution of the DTE approach tends to smooth out such local very intense fires. In regions 6 to 8, the DTE seasonal cycle starts too early and too rapidly compared to the other datasets. DTE and L3JRC, which starts one month ahead of GFED, agree better with each other. In region 7 (southern Angola/northern Namibia savannas), DTE shows the largest early bias. These three study regions correspond to areas in which forests (in particular, closed deciduous forests and mosaic forest/savanna) contribute the least (see for example, Fig. 2 of Mayaux et al. (2004)) compared to the other regions. Three tentative explanations of this early bias of DTE can be suggested. First, the DTE observation periods is 10 years earlier than GFEDv2, but neither Barbosa et al. (1999) nor Cooke et al. (1996) analyzing coinciding years, did report such an early fire season onset as found in DTE data. Second, advection of fire emissions laden air from northern Africa, a region with active fires in March, could contribute to the observed early DTE signal, given the seasonal winds direction (Edwards et al. 2003; Ryu and Jenkins 2005) ; however, this hypothesis would hardly match the diurnal cycle of the DTE. Third and perhaps more plausible, the early bias of DTE vs. GFEDv2/L3JRC may arise from limits of the burned area detection methods, especially for

detecting small burnt scars during the early season. Tansey et al. (2008b) report that the under detection bias of L3JRC product is more significant in areas of shrubs and grasses than over forests. Small but numerous fires are likely to be more frequent during the early fire season. Figure 10 also shows a remarkable agreement for region 10 (Madagascar), where land cover is fairly heterogeneous. For the ASn region, DTE is in phase with L3JRC, but GFEDv2 peaks one month later. For the ASs region, DTE shows a flat maximum from June to September whereas L3JRC peaks in August and GFEDv2 peaks in September. This earlier start of the DTE is consistent with the statement made by Swap et al. (2003) summarizing the main findings of the Southern African Regional Science Initiative SAFARI 2000: "In contrast to the commonly held understanding, the greatest areas burnt were recorded during June and July. The area burned during September comprised only 9% of the fire season total. These results indicate that the fire season peaks earlier than presumed (…) and contradicts the assumptions of several other investigators." An important point is that contamination of the DTE signal by either ozone or dust aerosols is expected to be small at that time of the year. Moreover, a detailed sensitivity analysis by Chédin et al., 2005 also concluded that only high altitude smoke aerosols (above 4 km) with high optical depths (> 0.7 at visible wavelengths, a maximum value found by Modis in August 2003) could contribute to the enhancement of the DTE signal by ~1 ppm.

In summary, there is a tight relationship between the seasonal cycles of DTE and of fire emission-related products. Despite this, DTE seems to have a systematically earlier onset than the two other products for regions 6 and 7 (and, to a lesser extent, 8), not yet satisfactorily elucidated.

4 Conclusions

The mid-troposphere diurnal anomaly observed by TOVS between evening and morning CO_2 columns (DTE) has been investigated at regional scale over southern Africa with the aim of analyzing its properties as a proxy of fire emission. A possible mechanism for CO_2 concentration being higher in the evening than in the morning is that hot convective fire plumes inject emissions directly into the troposphere during the afternoon peak of fire activity, seen by the satellite in the evening, and then diluted by large-scale atmospheric transport before the next satellite pass in the morning. 3D simulations described by Rio et al. (2009, this issue) and performed using the LMDz General Circulation Model including

a new pyro-thermal plume model essentially confirm the DTE magnitude and patterns deduced from the TOVS data:

(1) The pyro-thermal plume model injects a large fraction of fire products into the mid-troposphere, above the planetary boundary layer, where it can be seen by TOVS. Combined with the atmospheric circulation, this vertical transport leads to a daily DTE signal mostly positive over the source region, and either positive or negative outside, so that on a monthly mean basis a DTE signal of ~1ppm is obtained over regions affected by biomass burning. Although the simulations show that pyro-convection can transport CO_2 from fires in the mid-troposphere to produce a daily variation in CO_s, the observed DTE signal remains larger on average than the model simulations;

(2) The simulated and observed DTE distributions show a small number of negative values occurrences particularly south of 15S. This is likely due to the mean atmospheric circulation over southern Africa during the dry winter season, characterized by a semi permanent continental gyre prevailing approximately half of the time. This regional recirculation gyre may result in either negative DTE values or in abnormally positive values. Some compensation in the occurrence of negative and over-positive DTE values can maintain the quantitative relationship observed between DTE and emissions over fire regions.

Comparisons have then been made between the space and time variability of DTE and fire emission related products from the Global Fire Emission Database version 2 (GFEDv2) and global burnt areas database of the joint Research Center (L3JRC). Results obtained at seasonal, annual, interannual time-scales for 10 regions in southern Africa with contrasted vegetation cover have brought into evidence striking similarities between DTE and the other two products.

The main difference is a systematically earlier onset in the DTE compared to the two other products for essentially two regions in which forests (in particular, closed deciduous forests and mosaic forest/savanna) contribute the least compared to the other regions. This earlier DTE bias is not yet elucidated although a tentative explanation has been proposed based on the SAFARI 2000 experiment results presented by Swap et al. (2003) showing that fire scar estimates reveal contradictory information on the timing of the peak and extent of the biomass-burning season; this could possibly be due to the limits of the burned area detection methods for detecting small burnt scars during the early season. Also, one must

keep in mind that, for particularly intense fires, high altitude smoke aerosols can contribute to the enhancement of the DTE by about 1 ppm.

We conclude from this that DTE observations could probably prove useful to reconstruct fire emission patterns, in particular before the ATSR, SPOT or MODIS era and could also bring a constraint in the analysis of their present results.

Acknowledgements

This work has been supported in part by the European Community under the contract EVG1-CT-2001-00056 (''COCO'') and under the contract FP6-516099 (''GEMS''). Thanks are also due to the two anonymous referees for their constructive and helpful comments and criticism.

References

Aardenne van, J. A., Dentener, F. J., Olivier, J. G. J., Klein Goldewijk, C. G. M., and Lelieveld, J.: A 1°x1° resolution data set of historical anthropogenic trace gas emissions for the period 1890-1990, Global Change Biology, 15, 909-928, 2001.

Andreae, M. O.: Fire in the southern African Savanna: Ecological and Environmental Perspectives. B. W. van Wilgen et al. Eds. (Witwaterstrand University Press, Johannesburg), pp. 161-183, 1996.

Anyamba, A., Justice, C. O., Tucker, C. J., and Mahoney, R.: Seasonal to interannual variability of vegetation and fires at SAFARI 2000 sites inferred from advanced very high resolution radiometer time series data, J. Geophys. Res., 108, doi:10.1029/2002JD002464, 2003.

Archibald, S., Roy, D. P., van Wilgen, B. W., and Sholes, R. J.: What limits fire? An examination of drivers of burnt area in Southern Africa, Global Change Biology, 15, 613–630, doi: 10.1111/j.1365-2486.2008.01754, 2009

Barbosa, P. M., Stroppiana, D., Grégoire, J. M., and Pereira, J. M. C.: An assessment of vegetation fire in Africa (1981-1991): burned areas, burned biomass, and atmospheric emissions, Global Biogeochemical Cycles, 13, 933-950, 1999.

Bryant, R. G., Bigg, G. R., Mahowald, N. M., Eckardt, F. D., and Ross, S. G.: Dust emission response to climate in southern Africa, J. Geophys. Res., 112, D09207, doi:10.1029/2005JD007025, 2007.

Cahoon, D. R., Stocks, B. J., Levine, J. S., Coter III, W. R., and O'Neill, C. P.: Seasonal distribution of African savanna fires, Nature, 359, 812-815, 1992.

Chédin, A., Serrar, S., Armante, A., Scott, N. A., and Hollingsworth, A.: Signatures of annual and seasonal variations of CO_2 and other greenhouse gases from NOAA/TOVS observations and model simulations, J. Climate, 15, 95-116, 2002.

Chédin, A., Serrar, S., Scott, N. A., Crevoisier, C., and Armante, R.: First global measurement of mid-tropospheric CO_2 from NOAA polar satellites: the tropical zone, J. Geophys. Res., 108, doi:10.1029/2003JD003439, 2003a.

Chédin, A., Saunders, R., Hollingsworth, A., Scott, N.A., Matricardi, M., Etcheto, J., Clerbaux, C., Armante, R. and Crevoisier, C.: The feasibility of monitoring CO_2 from high resolution infrared sounders, J. Geophys. Res., 108, doi:10.1029/2001JD001443, 2003b.

Chédin, A., Serrar, S., Scott, N. A., Pierangelo, C., and Ciais, P.: Impact of tropical biomass burning emissions on the diurnal cycle of upper tropospheric CO_2 retrieved from NOAA-10 satellite observations, J. Geophys. Res., 110, doi:10.1029/2004JD005540, 2005.

Chédin, A., Scott, N. A., Armante, R., Pierangelo, C., Crevoisier, C., Fossé, O., and Ciais, P.: A quantitative link between CO_2 emissions from tropical vegetation fires and the daily tropospheric excess (DTE) of CO_2 seen by NOAA-10 (1987–1991), J. Geophys. Res., 113, doi:10.1029/2007JD008576, 2008.

Ciais, P., Piao, S.-L., Cadule, P., Friedlingstein, P., and Chédin, A.: Variability and recent trends in the African carbon balance, Biogeosci. Discuss., 5, 3497–3532, 2008.

Coheur, P.-F., Herbin, H., Clerbaux, C., Hurtmans, D., Wespes, C., Carleer, M., Turquety, S., Rinsland, C. P., Remedios, J., Hauglustaine, D., Boone, C. D., and Bernath, P. F.: ACE-FTS observation of a young biomass burning plume: first reported measurements of C_2H_4, C_3H_6O, H2CO and PAN by infrared occultation from space, Atmos. Chem. Phys., 7, 5437-5446, 2007.

Cooke, W., Koffi, B., and Grégoire, J. M.: Seasonality of vegetation fires in Africa from remote sensing data and application to a global chemistry model, J. Geophys. Res., 101, 21051-21065, 1996.

Crutzen, P. J. and Zimmermann, P. H.: The changing photochemistry of the troposphere, Tellus, 43AB, 136-151, 1991.

DeFries, R.S., Hansen, M., Townshend, J. R. G., and Sohlberg, R.: Global land cover classifications at 8km spatial resolution: the use of training data derived from Landsat imagery in decision tree classifiers, Int. J. Remote Sensing, 19, 3141-3168, 1998.

Duncan, B. N., Martin, R. V., Staudt, A. C., Yevich, R., and Logan, J. A.: Interannual and seasonal variability of biomass burning emissions constrained by satellite observations, J. Geophys. Res., 108, doi:101029/2002JD002378, 2003.

Freitas, S. R., Longo, K. M., and Andreae, M. O.: Impact of including the plume rise of vegetation fires in numerical simulations of associated atmospheric pollutants, Geophys. Res. Lett., 33, doi:10.1029/2006GL026608, 2006.

Freitas, S. R., Longo, K. M., Chattfield, R., Latham, D., Silva Dias, M. A., Andreae, M. O., Prins, E., Santos, J. C., Gielow, R., and Carvalho, J. A.: Including the sub-grid scale plume rise of vegetation fires in low resolution atmospheric transport models, Atmos. Chem. Phys., 7, 3385-3398, 2007.

Giglio, L., Csiszar, I., and Justice, C. O.: Global distribution and seasonality of active fires as observed with the Terra and Aqua Moderate Resolution Imaging Spectroradiometer (MODIS) sensors, J. Geophys. Res., 111, doi:10.1029/2005JG000142, 2006a.

Giglio, L., van der Werf, G. R., Randerson, J. T., Collatz, G. J., and Kasibhatla, P.: Global estimation of burned area using MODIS active fire observations, Atmos. Chem. Phys., 6, 957-974, 2006b.

Giglio, L.: Characterization of the tropical diurnal fire cycle using VIRS and MODIS observations, Remote Sensing of Environment, 108, doi:10.1016/j.rse.2006.11.018, 2007.

Hoelzemann, J. J., Schultz, M. G., Brasseur, G. P., Granier, C., and Simon, M.: The Global Wildland fire Emission Model GWEM: evaluating the use of global area burnt satellite data, J. Geophys. Res., 109, doi10.1029/2003003666, 2004.

Hoelzemann, J. J.: Global Wildland Fire Emission Modeling for Atmospheric Chemistry Studies, PhD thesis, Max Planck Institute for Meteorology / University of Hamburg, Germany, Reports on Earth System Science, 28/2006, ISSN 1614 -1199, 2006.

Hourdin, F., Musat, I., Bony, S., Braconnot, P., Codron, F., Dufresne, J. L., Fairhead, L., Filiberti, M.-A., Friedlingstein, P., Grandpeix, J.-Y., Krinner, G., LeVan, P., Li Z.-X., and Lott, F.: The LMDz4 general circulation model : climate performance and sensitivity to parametrized physics with emphasis on tropical convection, Climate Dynamics , *27* : 787-813, 2006.

Ito, A. and Penner, J. E.: Global estimates of biomass burning emissions based on satellite imagery for the year 2000, J. Geophys. Res., 109, doi:10.1029/2003JD004423, 2004.

Jury, M R.: The dry season climate of tropical southern Africa and implications for pyrogenic emissions, South African J. Sci., 96, 387-390, 2000.

Kasischke, E. S. and Penner, J. E.: Improving global estimates of atmospheric emissions from biomass burning, J. Geophys. Res., 109, doi:10.1029/2004JD004972, 2004.

Langenfelds, R. L., Francey, R. J., Pak, B. C., Steele, L. P., Lloyd, J., Trudinger, C. M., and Allison, C. E.: Interannual growth rate variations of atmospheric CO_2 and its $\delta^{13}C$, H_2, CH_4, and CO between 1992 and 1999 linked to biomass burning, Global Biogeochem. Cycles, 16, doi: 10129/2001GB001466, 2002.

Lehsten, V., Tansey, K., Balzter, H., Thonicke, K., Spessa, A., Weber, U., Smith, B., and Arneth, A.: Estimating carbon emissions from African wildfires, Biogeosciences, 6, 349–360, 2009.

Liousse, C., Guillaume, B., Grégoire, J.-M., Mallet, M., Galy, C., Pont, V., Solmon, F., Poirson, A., Rosset, R., Serca, D., Mariscal, A., Dungal, L., Yoboué, V., Bedou, X., Konaré, A., Granier, C., Mieville, A., and van Velthoven, P.: , submitted to ACPD, 2009.

Mayaux, P., Bartholomé, E., Fritz, S., and Belward, A.: A new land-cover map of Africa for the year 2000, J. Biogeogr., 31, 861–877, 2004.

Mouillot, F. and Field, C. D.: Fire history and the global carbon budget: a 1°x1° fire history reconstruction for the 20th century, Global Change Biology, 11, 398-420, 2005.

Palacios-Orueta, A., Chuvieco, E., Parra, A., and Carmona-Moreno, C.: Biomass burning emissions: a review of models using remote-sensing data, Environ. Monit. Assess., 104, 189-209, 2005.

Patra, P. K., Ishizawa, M., and Maksyutov, S.: Role of biomass burning and biomass anomalies for land-atmosphere carbon fluxes based on inverse modeling of atmospheric CO_2, Global Biogeochemical Cycles, 19, doi:10.1029/2004GB002258, 2005.

Potter, C. S., Randerson, J. T., Field, C. B., Matson, P. A., Vitousek, P. M., Mooney, H. A., and Klooster, S. A.: Terrestrial ecosystem production: A process-oriented model based on global satellite and surface data, Global Biogeochem. Cycles, 7, 811 – 842, doi:10.1029/93GB02725, 1993.

Randerson, J. T., Thompson, M. V., Conway, T. J., Field, C. B., and Fung, I. Y.: Substrate limitations for heterotrophs: Implications formodels that estimate the seasonal cycle of atmospheric CO_2, Global Biogeochem. Cycles, 10(4), 585–602, doi:10.1029/96GB01981, 1996.

Randerson, J.T., van der Werf, G. R., Collatz, G. J., Giglio, L., Still, C. J., Kasibhatla, P., Miller, J. B., White, J. W. C., DeFries, R. S., and Kasischke, E. S.: Fire emissions from C3 and C4 vegetation and their influence on interannual variability of atmospheric CO_2 and $d^{13}CO_2$. Global Biogeochemical Cycles, 19, doi:10.1029/2004GB002366, 2005.

Randerson, J. T., van der Werf, G. R., Giglio, L., Collatz, G. J., and Kasibhatla, P. S.: Global Fire Emissions Database, Version 2 (GFEDv2), available on-line (http://daac.ornl.gov/) from Oak Ridge National Laboratory Distributed Active Archive Center, Oak Ridge, Tennessee, U.S.A, 2006.

Rio, C., Hourdin, F., and Chédin, A.: Numerical simulation of tropospheric injection of biomass burning products by pyro-thermal plumes, submitted to Atmos. Chem. Phys. Discuss, 2009.

G. Roberts, G., Wooster, M. J., and Lagoudakis E.: Annual and diurnal african biomass burning temporal dynamics, Biogeosciences, 6, 849–866, 2009.

Rumelhart, D. E., Hinton, G. E., and Williams, R. J.: Parallel distributed processing: Explorations in the macrostructure of cognition, D. E. Rumelhart and McClelland, Eds. MIT Press, pp. 318-362, 1986.

Ryu, J.-H. and Jenkins, G. S.: Lightning-tropospheric ozone connections: EOF analysis of TCO and lightning data, Atmospheric Environ., 39, 5799–5805, 2005.

Schultz, M. G.: On the use of ATSR fire counts data to estimate the seasonal and interannual variability of vegetation fire emissions, Atmos. Chem. Phys., 2, 387-395, 2002.

Schultz, M. G., Wooster, M., Boucher, O., Doutriaux-Boucher, M., Granier, C., Heil, A., Hollingsworth, A., Kaiser, J. W., Kasilowski, T., Morcrette, J.-J., Roberts, G., Simmons, A., and van der Werf, G. R.: Evaluation of a fire radiative power product derived from Meteosat 8/9 and identification of operational use, Final Report, EUMETSAT contract EUM/CO/06/4600000277/YG, 139 pp, 2008.

Sinha, P., Hobbs, P. V., Yokelson, R. J., Blake, D. R., Gao, S., and Kirchstetter, T. W.: Distributions of trace gases and aerosols during the dry biomass burning season in southern Africa, J. Geophys. Res., 108, doi:10.1029/2003JD003691, 2003.

Smith, W. L., Woolf, H. M., Hayden, C. M., Wark, D. Q., and McMillin, L; M.: The TIROS-N Operational Vertical Sounder, Bull. Amer. Meteor. Soc., 60, 1177- 1187, 1979.

Swap, R. J., Annegarn, H, J., Suttles, J. T., King, M. D., Platnick, S., Privette, J. L., and Scholes, R. J.: Africa burning: A thematic analysis of the Southern African Regional Science Initiative (SAFARI 2000), J. Geophys. Res., 108, doi:10.1029/2003JD003747, 2003.

Tansey, K., Grégoire, J.-M., Defourny, P., Leigh, R., Pekel, J.-F., van Bogaert, E., and Bartholomé, E.: A new, global, multi-annual (2000–2007) burnt area product at 1 km resolution, Geophys. Res. Lett., 35, doi:10.1029/ 2007GL031567, 2008a.

Tansey, K., Beston, J., Hoscilo, A., Page, S. E., and Paredes Hernandez, C. U.: Relationship between MODIS fire hot spot count and burned area in a degraded tropical peat swamp forest in Central Kalimantan, Indonesia, J. Geophys. Res., 113, doi:10.1029/2008JD010717, 2008b.

Weber, U., Jung, M., Reichstein, M., Beer, C., Braakhekke, M. C., Lehsten, V., Ghent, D., Kaduk, J., Viovy, N., Ciais, P., Gobron, N., and Rödenbeck, C.: The interannual variability of Africa's ecosystem productivity: a multi-model analysis**,** Biogeosci., 6, 285-295, 2009.

Werf van der, G. R., Randerson, J. T., Collatz, G. J., and Giglio, L.: Carbon emissions from fires in tropical and subtropical ecosystems, Global Change Biology, 9, 547-562, 2003.

Werf van der, G. R., Randerson, J. T., Collatz, G. J., Giglio, L., Kasibhatla, P. S., Arellano Jr, A. F., Olsen, S. C., Kasischke, E. S.: Continental partitioning of fire emissions during the 1997 to 2001 El Nino/La Nina period, Science, 303, 73-76, 2004.

Werf van der, G. R., Randerson, J. T., Giglio, L., Collatz, G. J., Kasibhatla, P. S., and Arellano Jr., A. F.: Interannual variability in global biomass burning emissions from 1997 to 2004, Atmos. Chem. Phys., 6, 3423-3441, 2006.

Werf van der, G. R., Randerson, J. T., Giglio, L., Gobron, N., and Dolman, A. J.: Climate controls on the variability of fires in the tropics and subtropics, Global Biogeochem. Cycles, 22, doi:10.1029/2007GB003122, 2008.

Wittenberg, U., Heimann, M., Esser, G., David McGuire, A., and Sauf, W.: On the influence of biomass burning on the seasonal CO_2 signal as observed at monitoring stations, Global Biogeochem. Cycles, 12, 531-544, 1998.

Ziemke, J. R., Chandra, S., Duncan, B. N., Froidevaux, L., Bhartia, P. K., Levelt, P. F., Waters, J. W.: Tropospheric ozone determined from Aura OMI and MLS: Evaluation of measurements and comparison with the Global Modeling Initiative's Chemical Transport Model, J. Geophys. Res., 111, doi:10.1029/2006JD007089, 2006.

Table 1. Limits in latitude and longitude of the 10 regions used in this study (adapted from Hoelzemann et al. (2006)). The two regions ASn and ASs integrate the northern and the southern parts of southern Africa respectively.

region code	*latitude min*	*latitude max*	*longitude min*	*longitude max*
H1	-6	0	8	28
H2	-6	0	28	43
H3	-10	-6	10	28
H4	-10	-6	28	40
H5	-14	-10	10	28
H6	-14	-10	28	43
H7	-25	-14	10	20
H8	-25	-14	20	28

H9	-25	-14	28	40
H10	-25	-12	42	50
ASs	-25	-15	8	43
ASn	-15	0	8	43

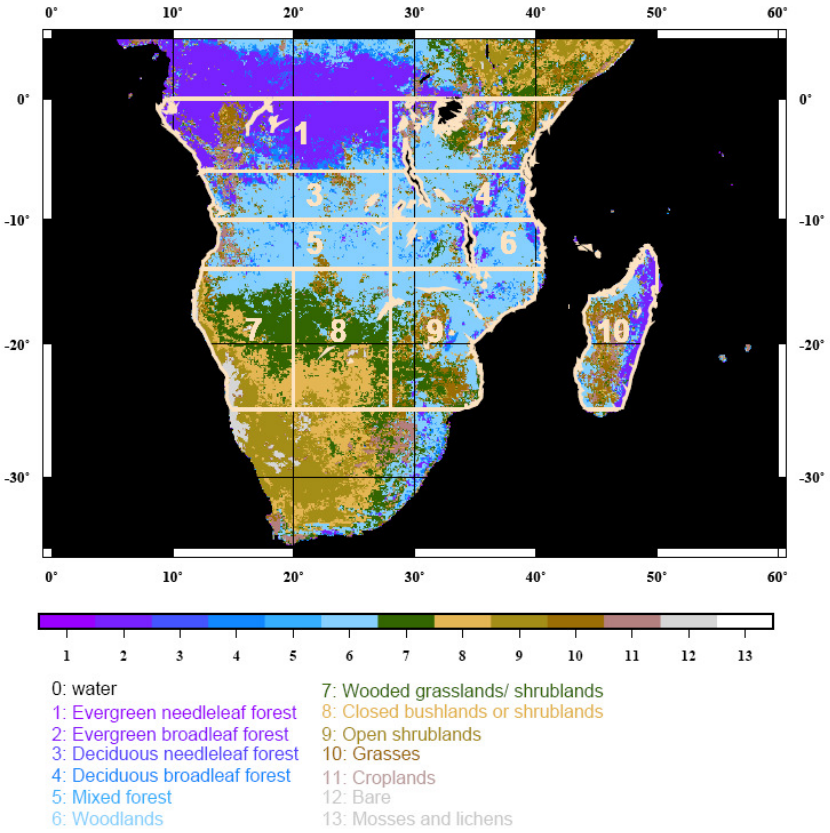

Figure 1: The 10 regions of the study adapted from Hoelzemann (2006). Note the change in the southern-most limit: 25S here, instead of 34S in the above reference. Vegetation map is from DeFries et al. (1998).

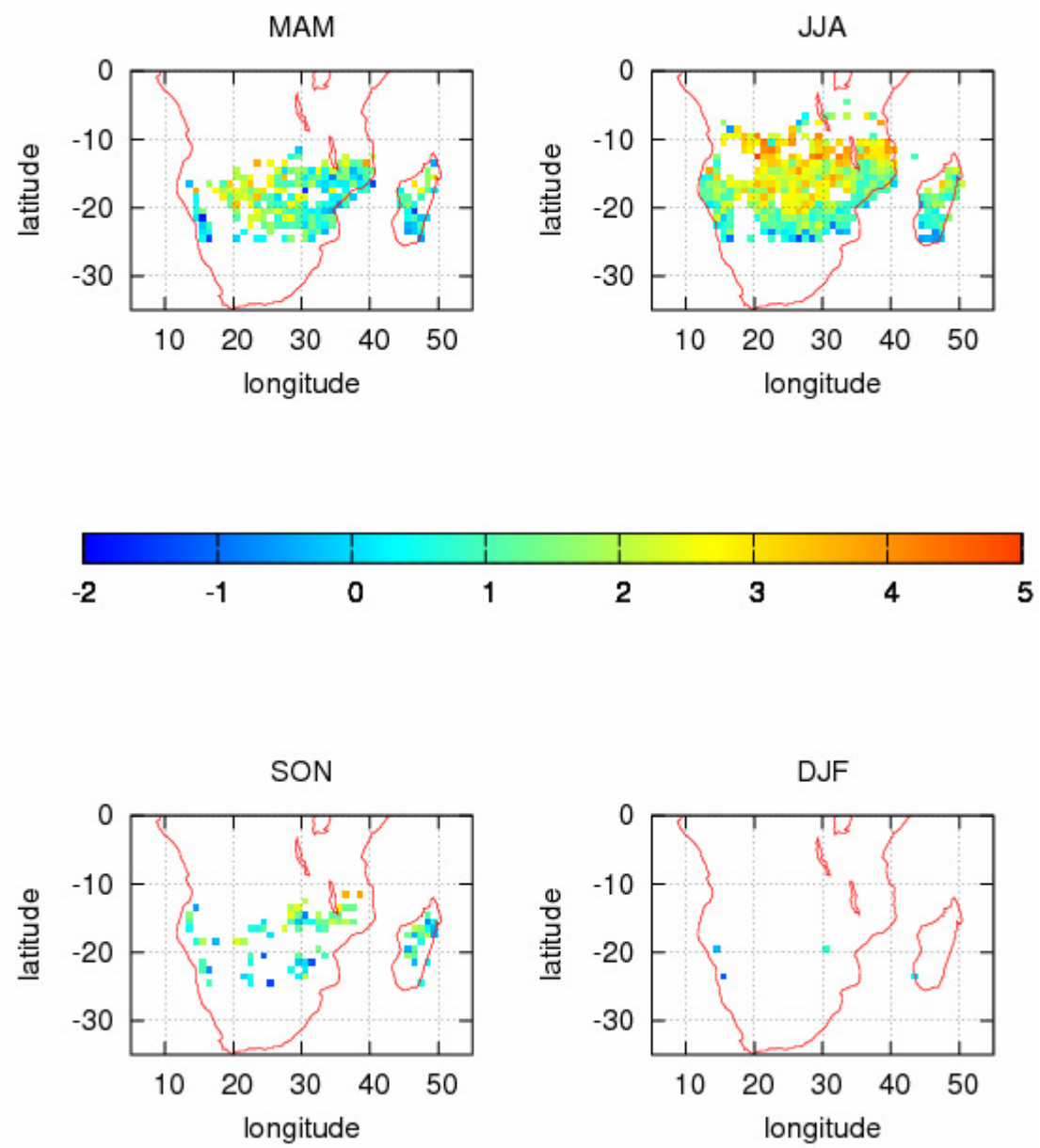

Figure 2: Four-year averaged seasonal maps of the DTE: (a) MAM; (b): JJA; (c) SON; (d): DJF.

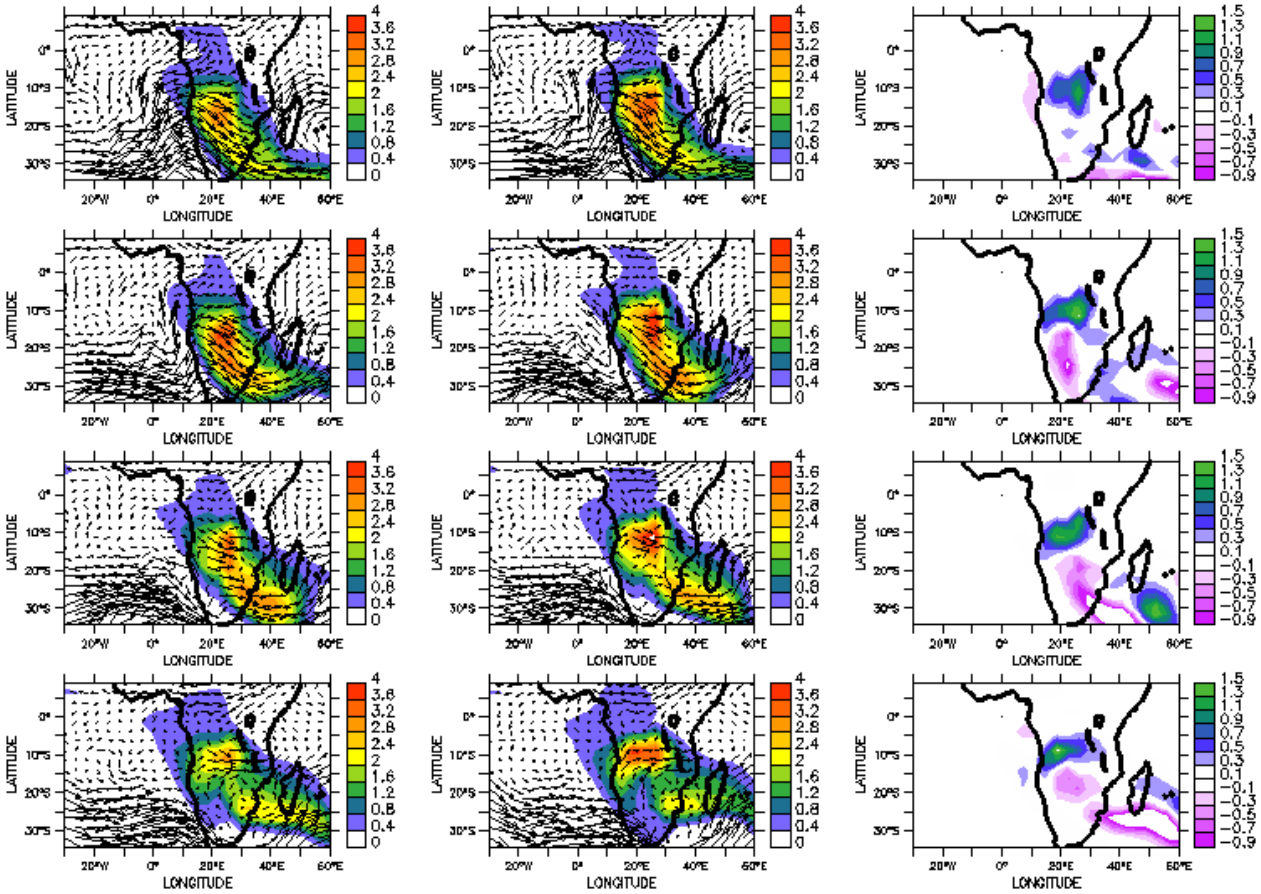

Figure 3: Simulated integrated CO_2 concentration from biomass burning which would be retrieved from satellite at 7am (left), and 7pm (middle) and the difference between the concentration at 7pm and the one at 7am (right), on (from top to bottom) the 18th , 19th, 20th and 21th of July. Horizontal winds at 500 hPa averaged over night are drawn upon the modelled CO_2 at 7am, and afternoon winds upon modelled CO_2 at 7pm.

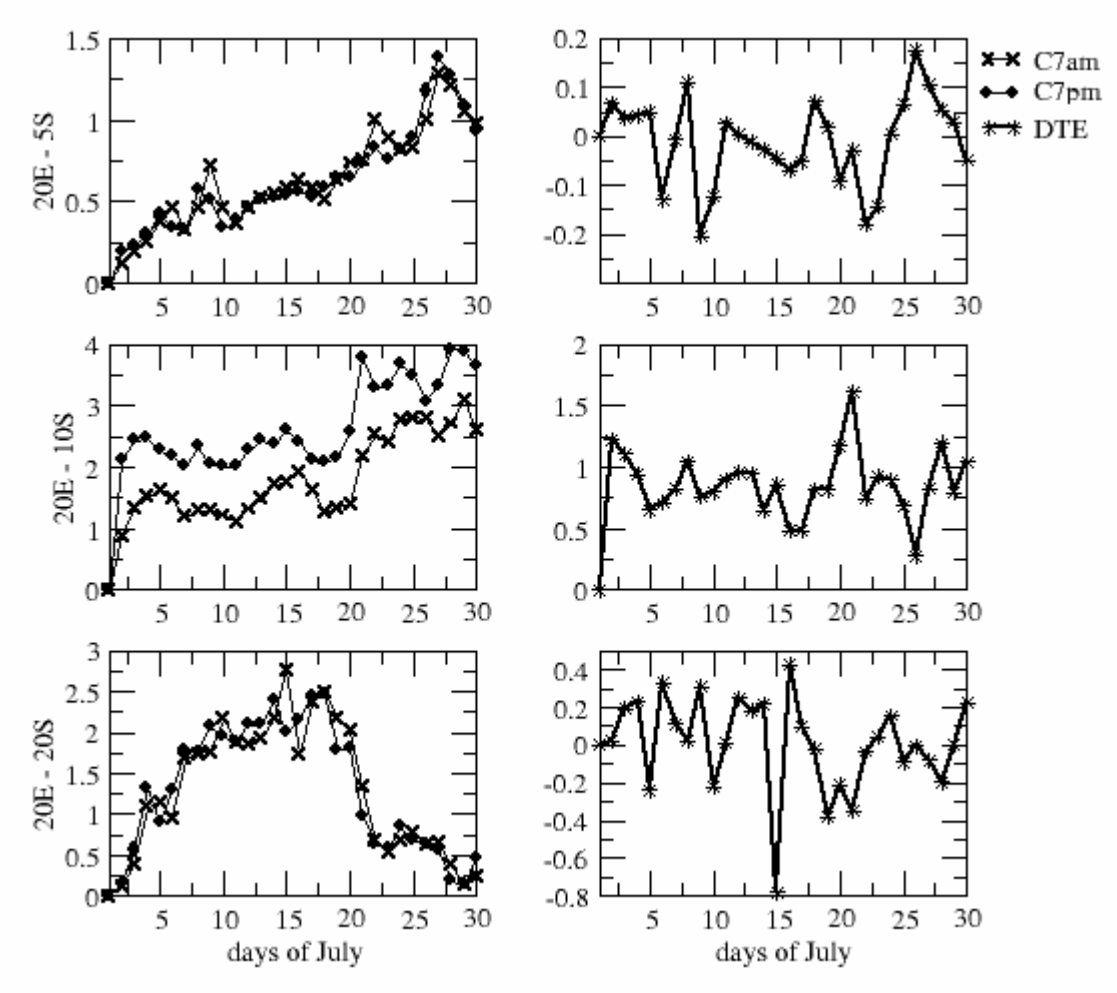

Figure 4: Monthly evolution of the simulated concentration as would be seen by the satellite at 7am and 7pm (left) and of the simulated DTE signal (right) at three different locations over Southern Africa, north of the source region (20E-5S), in the middle of the source region (20E-10S) and south of the source region (20E-20S), from top to bottom.

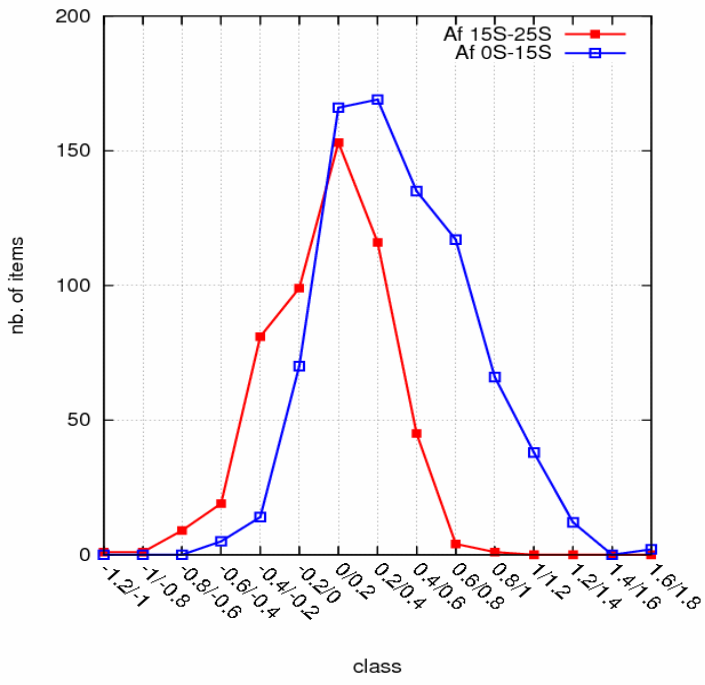

Figure 5: Distribution of the modelled DTE signal of July for regions Afn and Afs; class "0.2/0.4" is for DTE values ranging from 0.2 to 0.4 (in ppm).

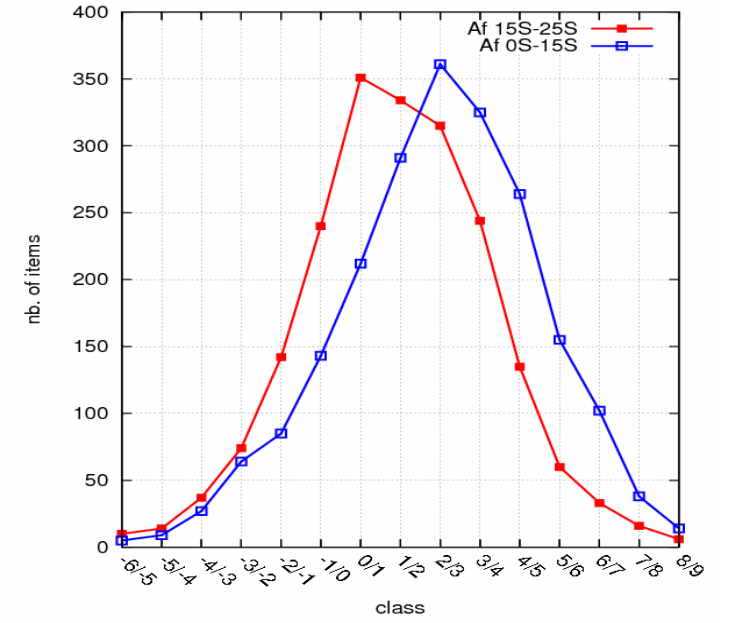

Figure 6: Histograms of the observed DTE for the season June, July, and August of the period 1987-1990; class "0/1" is for DTE values ranging from 0 to 1 (in ppm).

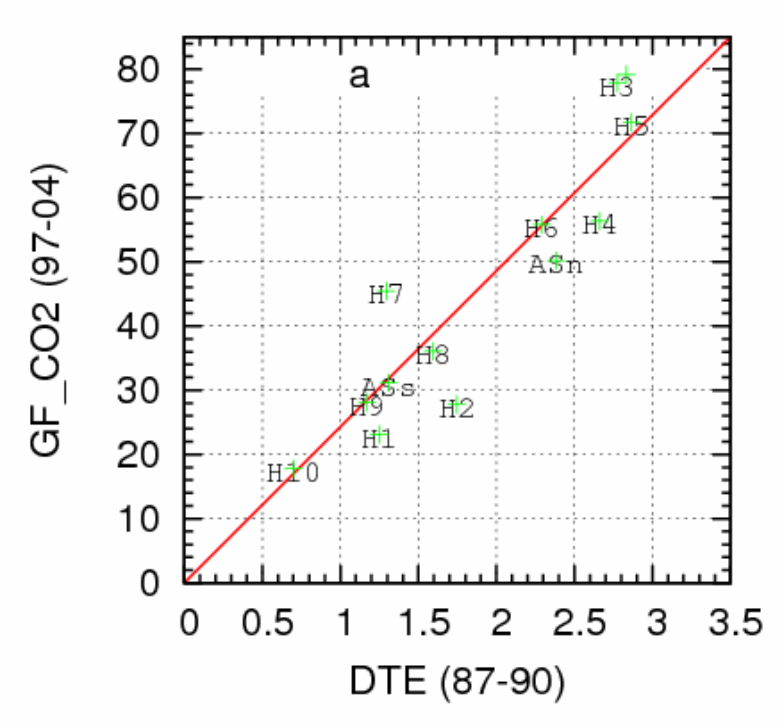

Figure 7: GFEDv2 CO_2 annual mean emissions (in g CO_2 m^{-2}) averaged over the period 1997-2004 (van der Werf et al., 2006) versus annual mean DTE (in ppm) averaged over the period 1987-1990 for the 10 regions of the study and the 2 integrated ASn and ASs regions.

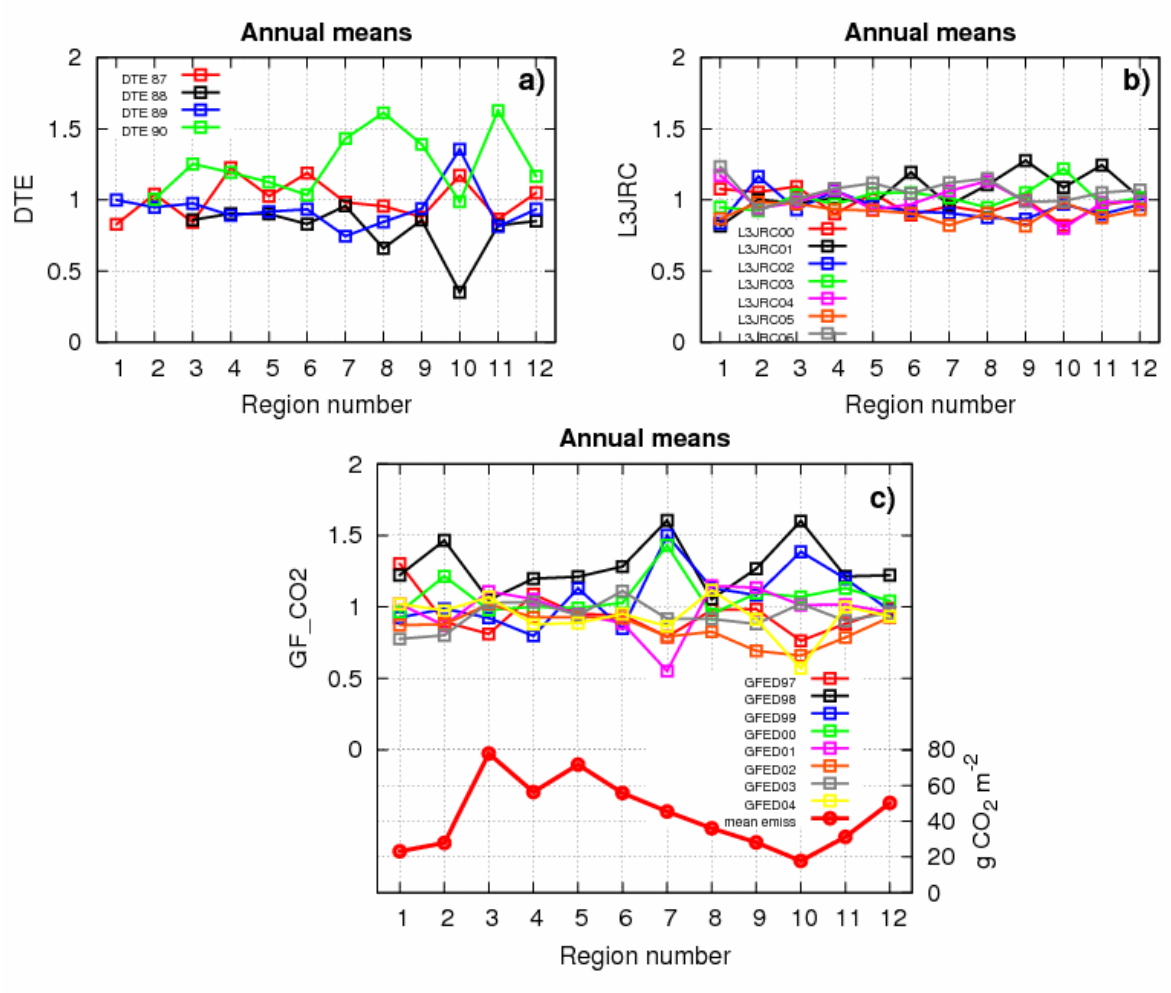

1

2

3 Figure 8: Annual means of DTE (a), L3JRC burned fractions (b), and GFED CO_2
4 emissions (c) for the regions of study, normalized by their mean over their respective time
5 periods: (1987-1990), (1997-2004), and (2000-2007). Missing data in Fig. 4a are due to too
6 small numbers of items available. The red dashed line in Fig. 4b shows the GFED CO_2
7 emissions (in g CO_2 m^{-2}) averaged over the period 1997-2004.

8

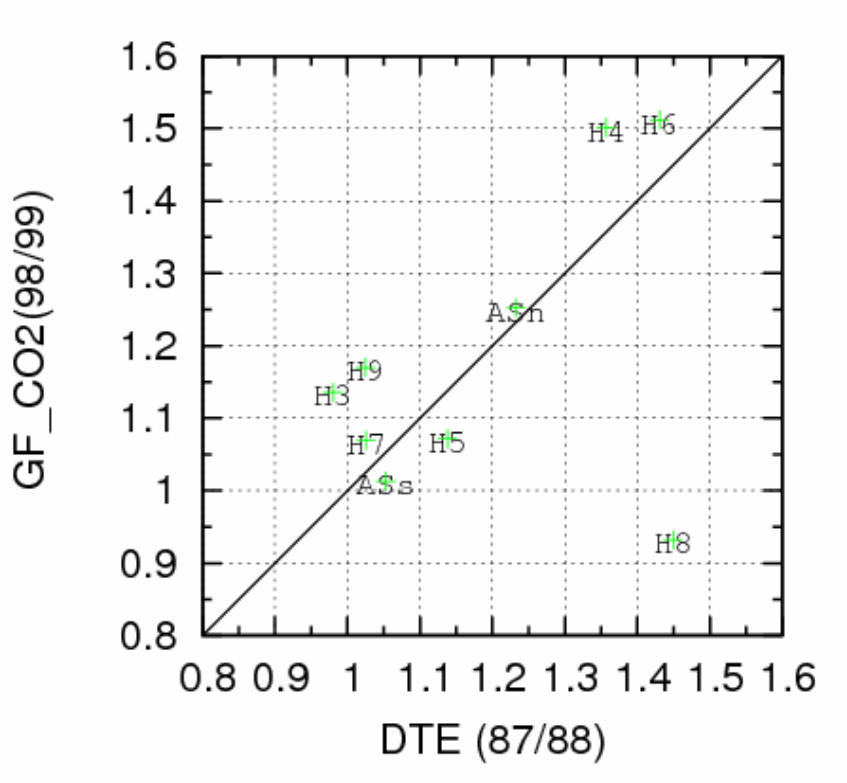

Figure 9: Ratio of emissions in 1998 to the emissions in 1999 in GFEDv2 versus the ratio of DTE in 1987 to 1988. The selected pairs of years are both composed of an El Nino year (1987 and 1998) and a La Nina year (1988 and 1999). Missing data are due to too small number of items available (regions 1 and 2) or to a result out of the graph (region 10; see text).

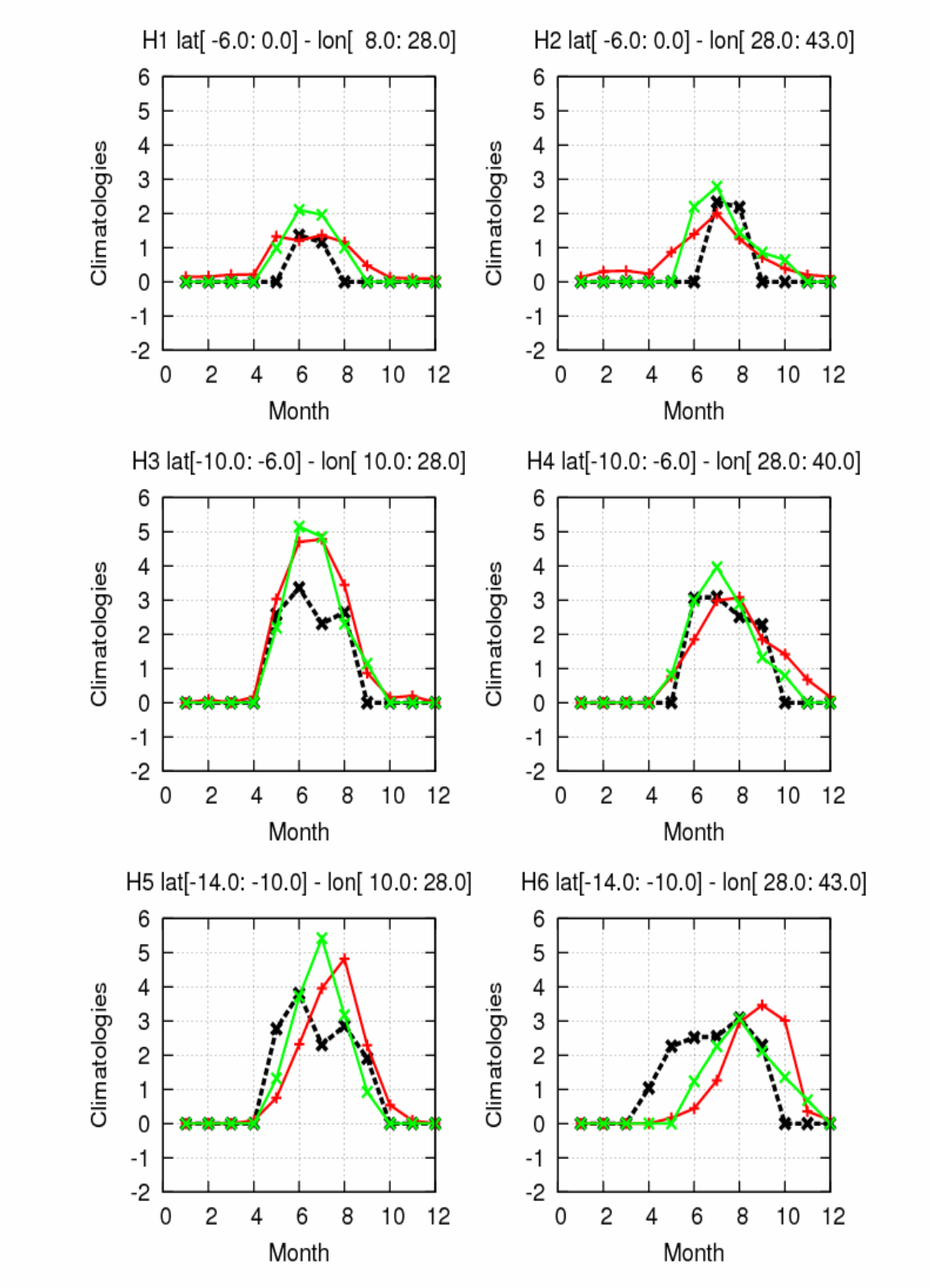

1

2 Figure 10: Seasonal cycles of: DTE (in ppm, averaged over 1987-1990, dashed black);
3 GFEDv2 CO_2 emission (in g CO_2 m^{-2}, averaged over 1997-2004, red); L3JRC burned
4 fraction (averaged over 2000-2007, green). Both GFED and L3JRC values have been
5 scaled to fit the DTE value range.

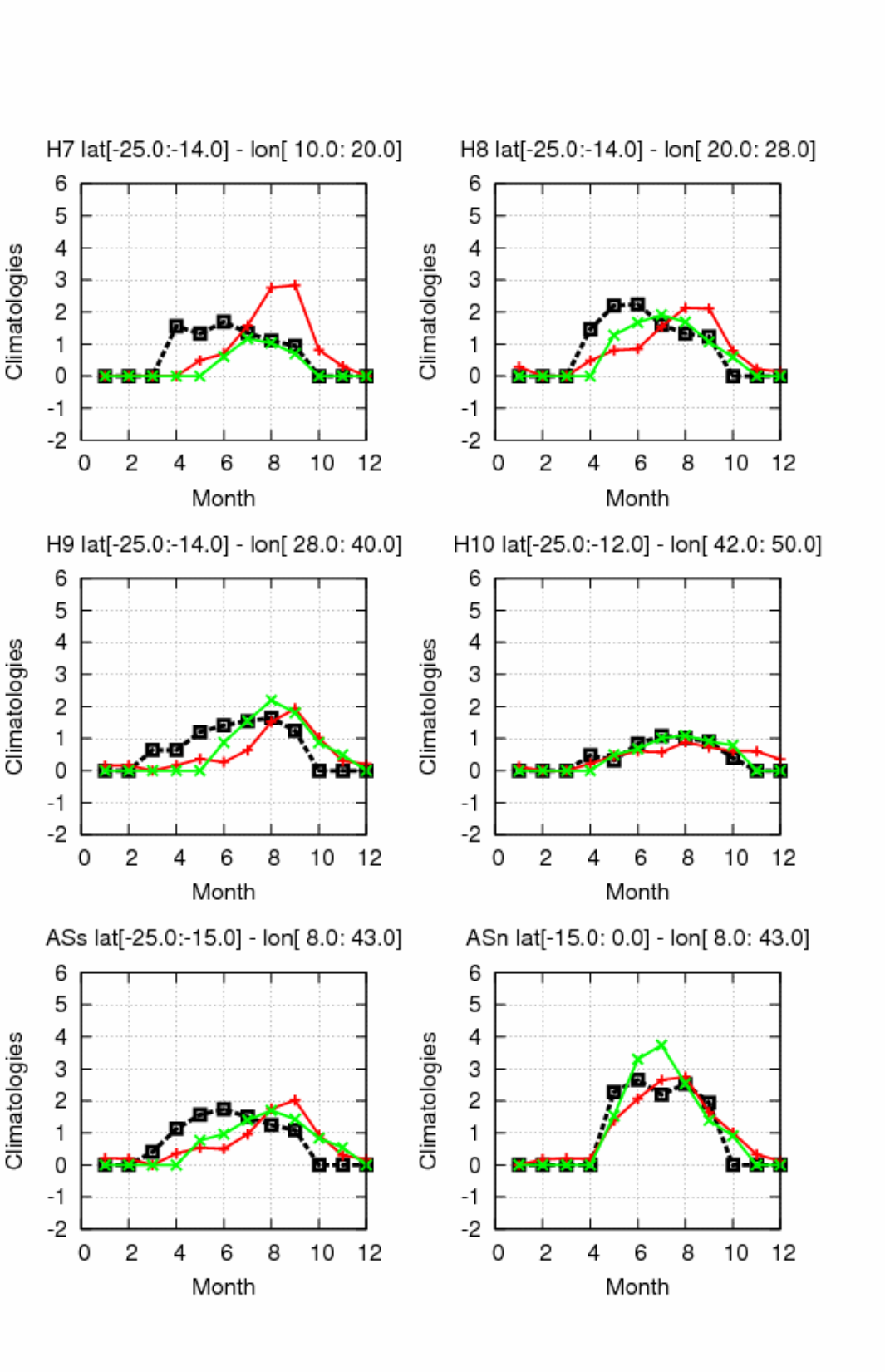

Figure 10: Continued